Effect of cutting tool geometry on hole quality in orbital drilling. Application to titanium alloy Ti-6Al-4V

Pierre-andre REY (pierre-andre.rey@ensam.eu)
Arts et Metiers ParisTech - Centre de Bordeaux-Talence
Johanna Senatore
Yann Landon

Research Article

Keywords: Orbital drilling, 3D chip geometry simulation, tool geometry optimization, Ti-6Al-4V

Posted Date: September 22nd, 2022

DOI: https://doi.org/10.21203/rs.3.rs-2017896/v1

Effect of cutting tool geometry on hole quality in orbital drilling. Application to titanium alloy Ti-6Al-4V

Pierre-André REY*[(1)], Johanna SENATORE [(2)], Yann LANDON [(2)]

[(1)] *Institut de mécanique et d'ingénierie, CNRS UMR 5295, Arts et Métiers ParisTech - Campus de Bordeaux, Esp. des Arts et Métiers, 33405 Talence*
[(2)]*Institut Clément Ader, CNRS UMR 5312, Université Paul Sabatier, 3 rue Caroline Aigle, 31400 Toulouse, France.*
** corresponding author :* pierre-andre.rey@ensam.eu

Abstract: The orbital drilling process is a very complex machining operation. Due to the helical path of the tool in the material and the sometimes very complex tool geometry, the geometry of the chip is very variable along the cutting edge and during a revolution of the tool. tool. This complexity explains why the cutting forces are very variable during drilling and they are very difficult to model and estimate for different tool geometries. The aim of this study is therefore to develop a cutting force model taking into account the geometry of the tool and the cutting conditions. The final objective is to control the final quality of the machined borehole. First, the geometry of the chip is modeled from the cutting parameters defining the trajectory and from the macro-geometry of the tool. Cutting force models, based on the instantaneous chip thickness and applied to the drilling, are then implemented. An experimental study validates the modeling by cutting force measurements carried out during orbital drilling tests. From this modeling, it is now possible to study the influence of the geometry of the cutting tool on the forces in order to control the loading on the tool and therefore the final quality of the drilling.

Keywords: Orbital drilling, 3D chip geometry simulation, tool geometry optimization, Ti-6Al-4V

1. Introduction

For mechanical assembly of structures, the realization of the fastening holes is an important matter. Especially in the aeronautical industry, the drilling process must reach high level requirements about hole quality, material integrity control, but also economical target in terms of productivity [1], [2]. It explains the constant interest brought to the drilling process by academic researchers as through industrial solution developments. According to the increasing diversity of materials used in aircraft structures, and their different characteristics, the process had to evolve to allow the drilling of holes in multi-material stacks made of highly different materials as composite laminates, titanium alloys, aluminium alloys... [3, 4]. A number of research studies have been brought on the characterization of new solutions in terms of cutting tools technologies and of processes as VAD [5, 6], or more recently the development of smart drilling [7]. Among these solutions can be cited the orbital drilling process. Orbital drilling, also called helical milling, involves making a hole with a tool of a diameter smaller than the diameter of the hole, driven on a helical path (Figure 1).

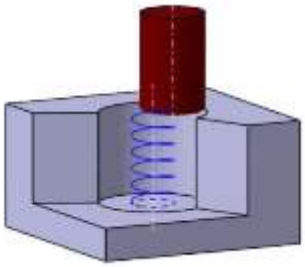

Figure 1 : Orbital drilling trajectory.

Developed at the beginning for wood drilling, it has been brought to industrial application for metal drilling and then composite drilling for different reasons. First it allows the drilling of different diameter holes with the same tool [4]. Also, the interrupted cutting process occurring in orbital drilling leads to a good chip fragmentation, and thus to an easier and improved chip evacuation through the radial gap between the tool and the borehole surface [8]. It can be added that this process generates low cutting forces that lead to a reduction of classical drilling defects as burrs in metallic materials or delamination in composite laminates [4, 9] [10]. Moreover, this process is also justified for drilling titanium alloys [11]. But its use has been also reduced because of the drilling duration and the more complex control of the trajectory (with tool deflection issue) [8]. Nevertheless, from a global economic point of view, the orbital drilling process may permit to reduce the number of operations to reach the finished borehole. In that case, it appears to be better to obtain the final hole in one operation of orbital drilling rather than in 2 or 3 operations of axial drilling and reaming. And considering the matter of trajectory programming, industrial solutions have been developed for this purpose, proposing orbital drilling units with an eccentric spindle [12]. The impact on the microstructure and the fatigue behaviour of drilled aerostructures was also studied, and Sun et al. [13] showed that orbital drilling has to be well optimized to reach the same level of fatigue behaviour the one obtain with axial drilling. After that, the control of the quality of the borehole quality has to be done through an optimization of the process: cutting conditions, and tool geometry [14]. Ozturk et al. [15] proposed a unified mathematical model which predicts three-dimensional chatter stability as a function of orbital pitch length, spindle speed and orbital speed of the tool and permits the optimization of the cutting conditions. Considering tool geometry, the influence of both axial and tangential feeds on borehole diameter quality has been investigated for simple flat-end tools [4, 16], based on a simple modelling of the chip geometry in orbital drilling with this simple-shape tools. For more complex tool geometries, another model of chip geometry and cutting forces was developed and proposed by Rey et al. [17] or more recently by Zhou et al. [18]. The tool geometry was introduced into the modelling by considering local cutting conditions (cutting speed gradient along the cutting edges) and forces. The tool geometry was firstly expressed analytically, before being divided into elementary edge portions. On each portion, a local cutting force model was applied. The elementary forces were then summed, according to the evolution of the edge geometry. Finally, this model makes it possible to simulate the geometry of the instantaneous chip and thus to have a 3D view of the material removal carried out. It also makes it possible to simulate the cutting forces as a function of the geometry of the tool considered, and to highlight the important role of the shape of the axial part of the tool. This allows for a better understanding of cutting phenomena in orbital drilling (e.g. deflection of the tool). In terms of applications, this model can be used to optimize the cutting conditions and the tool geometry in relation to the cutting forces generated (in direction and in amplitude). From the simulation of drilling defects due to the cutting forces (e.g. diameter decrease due to tool deflection), the model will permit to optimize the cutting conditions and/or the tool geometry in relation to the drilling quality. Based on this type of modelling, Zhou et al. [19] proposed an analysis of the chip-splitting performance of a dedicated cutting tool in dry orbital drilling. In this paper, this model is used to simulate the impact of different tool geometries in order to give a better understanding of the role of each part of the tool. A tool optimization is then possible. The results are discussed and compared to experimental tests for validation.

2. Kinematic modelling of orbital drilling

The modelling of the cutting forces by a semi-analytical approach requires precise knowledge of the geometry of the chips. To carry out a first model on the geometry of the chip, it is necessary to define the input data of this model as well as the references which will be used. The geometry of the tool, with the definition of the profile of the cutting edge as well as the cutting parameters are first defined. It is then the calculation of the instantaneous section of machined chip which is developed. In the present study, the drilling operation was simulated by down-milling but the model developed could also be used for up-milling.

2.1. Geometrical definition of orbital drilling

2.1.1. Definition of the tool geometry:

The tool macro-geometry (Figure 2) is defined using the following parameters:

Tool radius	R_t
Number of teeth	Z
Number of teeth with center-cut	Z_{cc}
Corner radius	R_b
Radius without center-cut	R_{cc}
Tool cutting edge angle	κ_r

Table 1: Geometrical parameters of the tool.

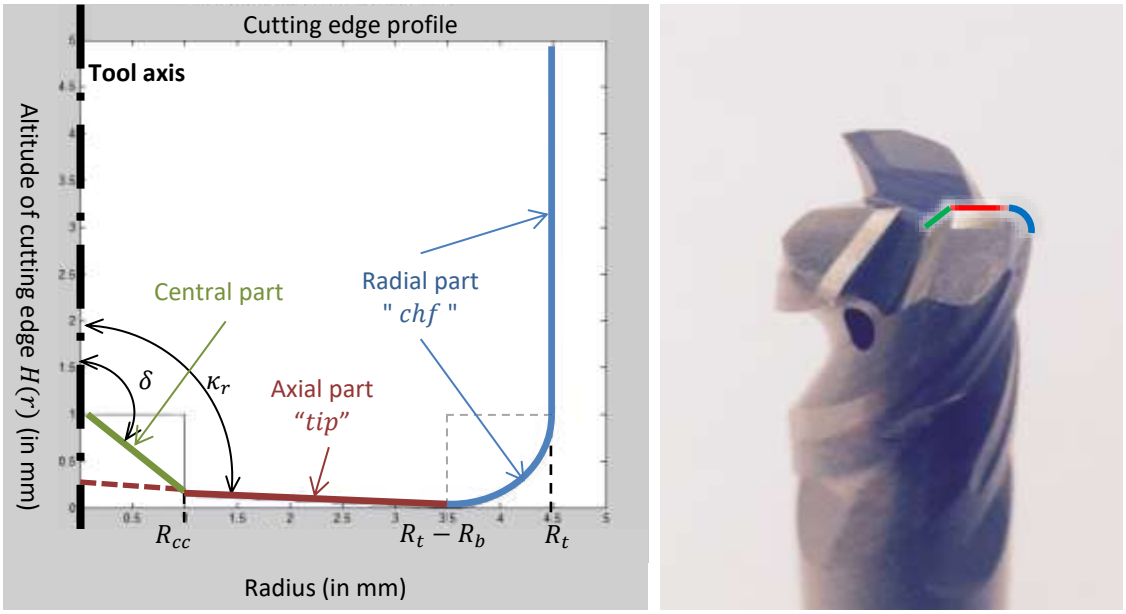

Figure 2 : Representation of the cutting edge profile.

Each edge is discretized into two parts: the radial part noted "chf", and the axial part noted "tip", which includes the central part when the latter is without center-cut.
A function $H(r)$ is established in order to define analytically the edge profile, it allows to give the altitude along the tool axis of each point of the edge versus radius r. The lowest tool point is defined at the altitude $Z = 0$. The function $H(r)$ is decomposed into several functions, to take into consideration the different parts of the edge:

- Central part if $0 < r < R_{cc}$:

$$H(r) = \left(R_{cc} - (R_t - R_b)\right) \times \tan\left(\frac{\pi}{2} - \kappa_r\right) + (R_{cc} - r) \times \tan\left(\delta - \frac{\pi}{2}\right)$$

With $\delta = \kappa_r$ in the case of the edge with center-cut (red dot line on Figure 2).

- Axial part (tip): if $R_{cc} < r < R_t - R_b$:

$$H(r) = [r - (R_t - R_b)].\, tan\left(\frac{\pi}{2} - \kappa_r\right)$$

- Radial part (chf) if $R_t - R_b < r < R_t$:

$$H(r) = R_b - \sqrt{{R_b}^2 - [r - (R_t - R_b)]^2}$$

2.1.2. Definition of cutting parameters:

The helical trajectory of the tool in orbital drilling can be decomposed into an axial feed f_a and a tangential feed f_t (Figure 3). The cutting parameters are thus presented in table 2.

Drilling radius	R_h
Interpolation radius, called offset	$R_{off} = R_h - R_t$
Pitch	P
Cutting speed	V_c
Tool revolution speed (rev/min)	$N = \frac{Vc}{2\pi \times R_t}$
Axial feed (mm/rev)	f_a
Axial feed per tooth (mm/tooth)	$f_{za} = \frac{f_a}{Z}$

Axial feed speed (mm/min)	$V_{fa} = f_a \times N$
Tangential feed (mm/rev)	f_t
Tangential feed per tooth (mm/rev/tooth)	$f_{zt} = \frac{f_t}{Z}$
Tangential feed speed (mm/min)	$V_{ft} = f_t \times N$
Orbital revolution speed	$N_{orb} = \frac{V_{ft}}{2\pi \times R_{off}}$

Table 2: Process parameters for orbital drilling.

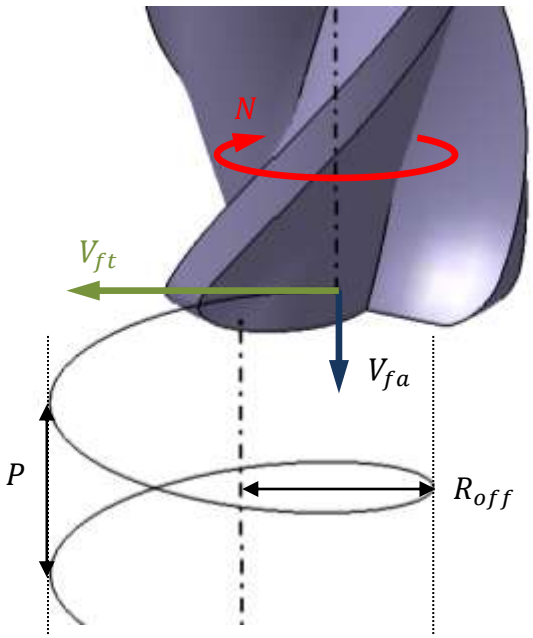

Figure 3 : Feed definition.

Now the geometrical parameters of the tool and the cutting conditions are defined, references need to be set to model the chip section.

2.1.3. References definition:

In this work, a local cutting force model is used. So it's necessary to define a local reference to calculate the elementary cutting forces on the cutting edge. These elementary forces obtained are then added together in order to simulate the overall resulting cutting forces, it is therefore necessary to define other references to express the resulting forces in the tool and machine reference. The index "i" is used to define the position of the tool on the orbital trajectory. Firstly, two characteristic points of the tool trajectory are defined:

- CL_i : the tool center location for the position "i".
- HL_i : the borehole center at the same altitude than CL_i.

The distance between HL_i and CL_i has been defined as the interpolation radius R_{off}.
Several references are then defined (figure 4):

- Machine reference: this reference is fixed in rotation.

$$R_m = (HL_i, \boldsymbol{X}, \boldsymbol{Y}, \boldsymbol{Z})$$

- Orbital reference: this reference permits to define the tool position "i" on the helical trajectory. This reference is described by the tool angular position θ_i in relation to the machine reference.

$$R_{oi} = (HL_i, \boldsymbol{X_{oi}}, \boldsymbol{Y_{oi}}, \boldsymbol{Z})$$

$$\text{With: } \begin{vmatrix} \boldsymbol{X_{oi}} = cos\,\theta_i.\boldsymbol{X} + sin\,\theta_i.\boldsymbol{Y} \\ \boldsymbol{Y_{oi}} = -sin\,\theta_i.\boldsymbol{X} + cos\,\theta_i.\boldsymbol{Y} \end{vmatrix} \quad \text{and} \quad \theta_i = (\boldsymbol{X}, \boldsymbol{X_{oi}})$$

- Tool reference: This local reference describes the angular position φ_i of the considered point of the tool in the tool revolution.

$$R_t = (CL_i, \boldsymbol{X_{ci}}, \boldsymbol{Y_{ci}}, \boldsymbol{Z})$$

With: $\left| \begin{matrix} \boldsymbol{X_{ci}} = cos\,\varphi_i.\boldsymbol{X_{oi}} + sin\,\varphi_i.\boldsymbol{Y_{oi}} \\ \boldsymbol{Y_{ci}} = -sin\,\varphi_i.\boldsymbol{X_{oi}} + cos\,\varphi_i.\boldsymbol{Y_{oi}} \end{matrix} \right.$ and $\varphi_i = (\boldsymbol{X_{oi}}, \boldsymbol{X_{ci}})$

The tool center location CL_i is defined with the offset:

$$\boldsymbol{HL_iCL_i} = R_{off}.\boldsymbol{X_{oi}}$$

The derivation of the angle φ_i is the tool revolution speed *N*.

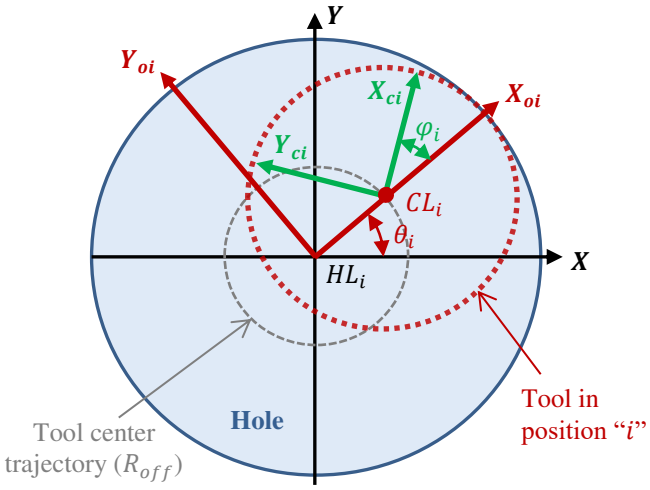

Figure 4 References definition.

The geometrical parameters of the orbital drilling operation and the references have been defined, now the calculation of the instantaneous chip section can be developed.

2.2. Calculation of the instantaneous machined chip section

As the cutting speed is largely higher than the tool feed speed, two simplifying assumptions are made:

- The tooth trajectory is considered circular (cycloid effect neglected), according to Segonds et al. [20].
- The calculation of the volume of the chip machined by the tool at each instant is the result of a Boolean subtraction operation between the volume of the machined work piece at the previous instant and the volume generated by the tool revolution at the position "i".

Therefore, to calculate the chip section machined by a tooth in position "i", two calculation steps are made. First, each point A_i belonging to the envelope surface of the tool in position "i" is described in R_{oi} in function of the radius $\|\boldsymbol{CL_iA_i}\| = r_{Ai}$ ($r_{Ai}\epsilon[0, R_t]$), φ_i ($\varphi_i\epsilon[0,2\pi]$) and $H(r)$ applied at the tool position "i":

$$\boldsymbol{CL_iA_i} = \begin{Bmatrix} r_{Ai} \\ 0 \\ Z_{Ai}(r_{Ai}, \varphi_i) = H(r_{Ai}) \end{Bmatrix}_{R_{ci}} = \begin{Bmatrix} X_{Ai}(r_{Ai}, \varphi_i) = r_{Ai}.cos\,\varphi_i \\ Y_{Ai}(r_{Ai}, \varphi_i) = r_{Ai}.sin\,\varphi_i \\ H(r_{Ai}) \end{Bmatrix}_{R_{oi}} \quad \text{(eq.1)}$$

The set of points A_i for a constant φ_i represents the edge where the chip section is assessed on.
Then, to calculate the section of the chip, it is necessary to identify the location of the previously machined surface above each point A_i. For this, all the locations of the tool that are before location "i" on a complete orbital revolution are considered. Each considered previous location is identified by its tool center point CL_k.
The difference of altitude following $\boldsymbol{Z}$ between two tool locations CL_i and CL_k is noted H_{ki}. Knowing that the tool describes a helical trajectory characterized by its pitch P (Figure 3), the height H_{ki} is defined according to the relative angular position θ_{ki} of both tool positions "i" and "k" (Figure 5):

$$H_{ki}(\theta_{ki}) = P - \frac{P \times \theta_{ki}}{2 \times \pi} \quad \text{(eq.2)}$$

The function H_{ki} is defined such as the tool location "k" is above the tool location "i" on the helical trajectory when the angle θ_{ki} is equal to zero.
Then, for each point A_i, the set of points A_k above A_i is identified in the reference R_{oi} as:

$$\boldsymbol{CL_iA_k} = \left\{ \begin{matrix} X_{Ak} = X_{Ai}(r_{Ai}, \varphi_i) \\ Y_{Ak} = Y_{Ai}(r_{Ai}, \varphi_i) \\ Z_{Ak} = H(r_{Ak}) + H_{ki}(\theta_{ki}) \end{matrix} \right\}_{R_{oi}} \quad \text{(eq.3)}$$

To calculate Z_{Ak}, the radius r_{Ak} has to be previously determined. For this purpose, the radius r_{ki}, which represents the radial position of the points A_i and A_k in the reference R_m, and the angle $\alpha = (\boldsymbol{HL_iCL_i}, \boldsymbol{HL_iA_i})$ have to be calculated first. They can be expressed by considering the triangle (HL_i, CL_i, A_i) (Figure 5):

$$r_{ki}(r_{Ai}, \varphi_i) = \sqrt{\left| {r_{Ai}}^2 + {R_{off}}^2 - 2 \times R_{off} \times r_{Ai} \times cos(\pi - \varphi_i) \right|} \quad \text{(eq.4)}$$

$$\alpha(r_{Ai}, \varphi_i) = cos^{-1}\left(\frac{{r_{ki}}^2 + {R_{off}}^2 - {r_{Ai}}^2}{2 \times r_{ki} \times R_{off}} \right) \quad \text{(eq.5)}$$

From Figure 5, considering the triangle (HL_i, CL_k, A_k), the expression of r_{Ak} can be deduced:

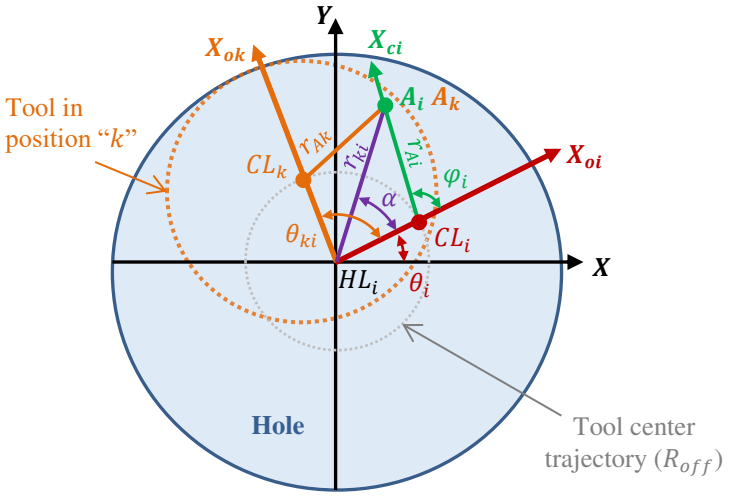

Figure 5 Locating a tool position "k" in relation to the tool position "i".

$$r_{Ak}(r_{Ai}, \varphi_i, \theta_{ki}) = \sqrt{\left| {r_{ki}}^2 + {R_{off}}^2 - 2 \times R_{off} \times r_{ki} \times cos(\theta_{ki} - \alpha) \right|} \quad \text{(eq.6)}$$

The set of points A_k related to every tool location "k" of the previous orbit revolution are calculated for each point A_i considered. To determine the location of the machined surface above A_i, the corresponding point A_k with the lowest altitude is kept and noted S_i.

$$\boldsymbol{CL_iS_i} = \left\{ \begin{matrix} X_{S_i}(r_{Ai}, \varphi_i) = X_{Ak} = X_{Ai} \\ Y_{S_i}(r_{Ai}, \varphi_i) = Y_{Ak} = Y_{Ai} \\ Z_{S_i}(r_{Ai}, \varphi_i) = \min\limits_{0 \le \theta_{ki} \le 2\pi}(Z_{Ak}) \end{matrix} \right\}_{R_{oi}} \quad \text{(eq.7)}$$

For a given tool position "i", the set of points S_i associated to the set of points A_i describes the previous machined surface. It permits to calculate the chip height on each point of the tool:

$$\boldsymbol{A_iS_i.Z} = Z_{S_i}(r_{Ai}, \varphi_i) - Z_{A_i}(r_{Ai}, \varphi_i) \quad \text{(eq.8)}$$

Along a cutting edge, the chip section is then obtained by plotting the set of points A_i and the associated points S_i, for a fixed angle φ_i (representing a tooth of the tool) and for $r_{Ai} \epsilon [0, R_t]$ (Figure 6). The chip section obtained is discretized into trapezoids. The decomposition is considered to be sufficiently thin, to be able to approximate each trapezoidal surface by a rectangular surface characterized by two values: its thickness h_i and its width b_i. The thickness h_i is considered normal to the edge profile.

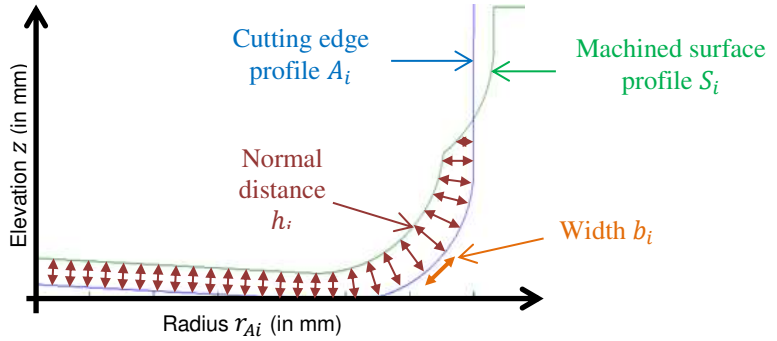

Figure 6 : Decomposition of the chip section.

From this calculation of the instantaneous chip sections it is possible to simulate the three-dimensional geometry of the chips obtained on a tool revolution. (Figure 7: see interactive figure in the online version).

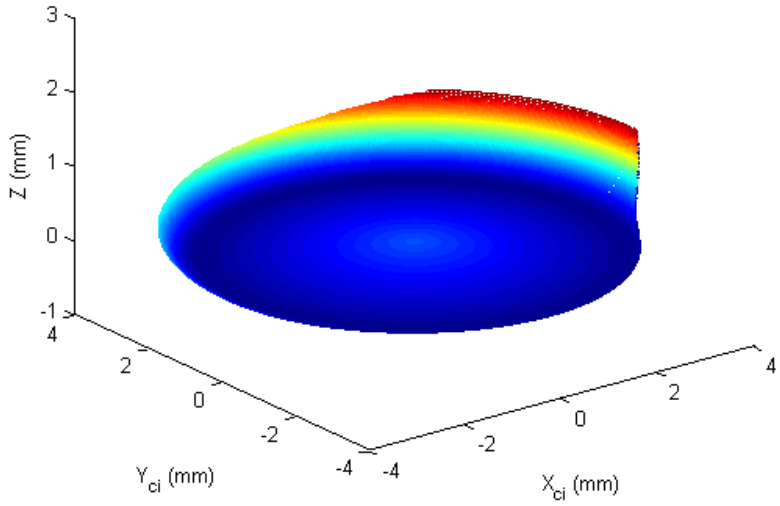

Figure 7: 3D visualisation of the chip (V_c=30m/min; f_z_a=0.005mm/tooth; f_z_t=0.04mm/tooth)

3. Cutting forces modelling

In this work a semi-analytical cutting model is chosen, as it permits to reduce the number of coefficients and calibration tests [21] [22]. Knowing the instantaneous chip section, the cutting forces applied on the tool during drilling can be expressed. This section of chip is discretized along the cutting edge making it possible to calculate the local forces "dF" on each discrete element:

$$dF = K^*.h.b \quad \text{(eq.9)}$$

Where K^* is a specific cutting coefficient. As the thickness of the chip (h_i) is highly variable, the specific cutting coefficient is considered non-constant [23] [24] and estimated by the following function [25]**:**

$$K^* = K.h^{-q} \quad \text{(eq.10)}$$

With K and q two constants.

Applying this model to each discrete element, three elementary forces applied on the tool are defined (Figure 8):

$$\begin{cases} dF_c = K_c.{h_i}^{1-q_c}.b_i \\ dF_n = K_n.{h_i}^{1-q_n}.b_i \\ dF_t = K_t.{h_i}^{1-q_t}.b_i \end{cases} \quad \text{(eq.11)}$$

Where h_i and b_i are dependent on the angular positionφ_i and on the radius r_{Ai}.

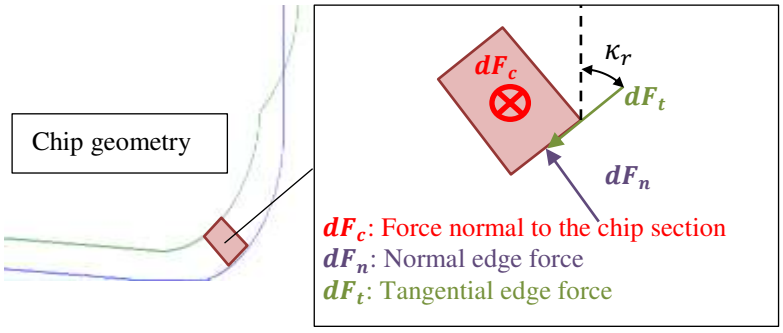

Figure 8 : Local forces applied on the tool for a given chip section.

It was previously defined that the cutting edge of the tool would be broken down into 2 parts; the axial part (also containing the central part and noted "tip") and the radial part (noted "chf") (Figure 2). On these parts, the geometry of the chip during the revolution of the tool is very different. The cutting conditions (cutting speed) are also variable along the cutting edge. Therefore the cutting mechanisms can be different in these different parts. This is the reason why the modelled cutting forces on the axial part of the tool and on its radial part are so considered separately. The corresponding cutting parameters K and q are also identified separately with specific calibration tests. The modelling of the cutting forces becomes:

- if $0 \leq r \leq R_t - R_b$:

$$\begin{cases} dF_c = dF_{c\_tip}(r_{Ai}, \varphi_i) = K_{c\_tip}.h_i(r_{Ai}, \varphi_i)^{1-q_{c\_tip}}.b_i(r_{Ai}, \varphi_i) \\ dF_n = dF_{n\_tip}(r_{Ai}, \varphi_i) = K_{n\_tip}.h_i(r_{Ai}, \varphi_i)^{1-q_{n\_tip}}.b_i(r_{Ai}, \varphi_i) \\ dF_t = dF_{t\_tip}(r_{Ai}, \varphi_i) = K_{t\_tip}.h_i(r_{Ai}, \varphi_i)^{1-q_{t\_tip}}.b_i(r_{Ai}, \varphi_i) \end{cases} \quad \text{(eq.12)}$$

- if $R_t - R_b < r \leq R_t$:

$$\begin{cases} dF_c = dF_{c\_chf}(r_{Ai}, \varphi_i) = K_{c\_chf}.h_i(r_{Ai}, \varphi_i)^{1-q_{c\_chf}}.b_i(r_{Ai}, \varphi_i) \\ dF_n = dF_{n\_chf}(r_{Ai}, \varphi_i) = K_{n\_chf}.h_i(r_{Ai}, \varphi_i)^{1-q_{n\_chf}}.b_i(r_{Ai}, \varphi_i) \\ dF_t = dF_{t\_chf}(r_{Ai}, \varphi_i) = K_{t\_chf}.h_i(r_{Ai}, \varphi_i)^{1-q_{t\_chf}}.b_i(r_{Ai}, \varphi_i) \end{cases} \quad \text{(eq.13)}$$

3.1. Modelling the cutting forces applied on the axial part of the tool

On the axial part of the tool, the above-mentioned modelling is applied on each tooth of the tool. To obtain the total cutting forces for the tooth "z" in position φ_i, the elementary cutting forces are summed along the edge:

$$\begin{cases} F_{c\_tip\,z}(\varphi_i) = \sum_{r_{Ai}=0}^{Rt-Rb} dF_{c\_tip\,z}(r_{Ai}, \varphi_i) = K_{c\_tip}.\sum_{r_{Ai}=0}^{Rt-Rb} h_i(r_{Ai}, \varphi_i)^{1-q_{c\_tip}}.b_i(r_{Ai}, \varphi_i) \\ F_{n\_tip\,z}(\varphi_i) = \sum_{r_{Ai}=0}^{Rt-Rb} dF_{n\_tip\,z}(r_{Ai}, \varphi_i) = K_{n\_tip}.\sum_{r_{Ai}=0}^{Rt-Rb} h_i(r_{Ai}, \varphi_i)^{1-q_{n\_tip}}.b_i(r_{Ai}, \varphi_i) \\ F_{t\_tip\,z}(\varphi_i) = \sum_{r_{Ai}=0}^{Rt-Rb} dF_{t\_tip\,z}(r_{Ai}, \varphi_i) = K_{t\_tip}.\sum_{r_{Ai}=0}^{Rt-Rb} h_i(r_{Ai}, \varphi_i)^{1-q_{t\_tip}}.b_i(r_{Ai}, \varphi_i) \end{cases} \quad \text{(eq.14)}$$

These cutting forces $F_{c\_tip\,z}(\varphi_i)$, $F_{n\_tip\,z}(\varphi_i)$ and $F_{t\_tip\,z}(\varphi_i)$ are calculated for each tooth of the tool, taking into account the differences in the tooth profile which can exist (with or without center-cut) (Figure 9).

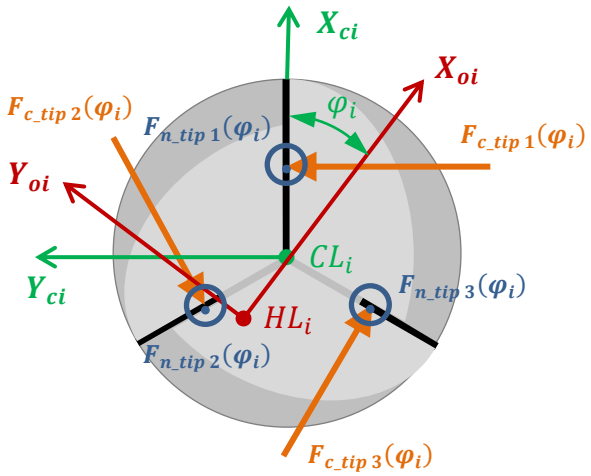

Figure 9 : Representation of forces generated on the axial part of a tool with three teeth (forces $F_{n\_tip\,z}(\varphi_i)$ are represented perpendicular to the figure).

For each tooth, the cutting force $F_{c\_tip\,z}(\varphi_i)$ applied on the axial part is normal to the chip section. Due to a local rake angle which is null, this force is included in the plane $(\boldsymbol{X_{ci}};\boldsymbol{Y_{ci}})$, or $(\boldsymbol{X_{oi}};\boldsymbol{Y_{oi}})$. The normal edge force $F_{n\_tip\,z}(\varphi_i)$ is included in the plane perpendicular to the cutting force $F_{c\_tip\,z}(\varphi_i)$, and nearly to be perpendicular to the edge. The tangential edge force $F_{t\_tip\,z}(\varphi_i)$ is also included in the plane perpendicular to the cutting force $F_{c\_tip\,z}(\varphi_i)$, and nearly to be tangent to the cutting edge.

For this cutting force model related to the axial part of the tool, 6 axial cutting parameters have to be identified: K_{c_tip}, K_{n_tip}, K_{t_tip} and q_{c_tip}, q_{n_tip}, q_{t_tip}. These parameters are considered to be the same for each tooth.

These force components only consider cutting mechanisms. But specific mechanisms may occur under the centre of the tool, as degraded cutting mechanisms or extrusion. To take into account this phenomenon into the modelling, an axial indentation force is added to the model. The selected modelling is the one proposed by Williams for axial drilling [26]:

$$F_{ind} = K_{ind}.{V_{fa}}^{q_{ind}}.S \qquad \text{(eq.15)}$$

Where S is the projected surface of the indentation zone under the centre of the tool. For a given tool, S can be considered as a constant since the axial feed speed remains low [6, 26]. This is especially the case in orbital drilling. Thus this parameter can be included into the coefficient K_{ind}.

3.2. Modelling the cutting forces applied on the radial part of the tool

On the radial part of the tool ("*chf*"), the modelling proposed (eq.13) for elementary forces $dF_{c\_chf\,z}(\varphi_i)$, $dF_{n\_chf\,z}(\varphi_i)$ and $dF_{t\_chf\,z}(\varphi_i)$, is applied for each tooth "z" (Figure 10).

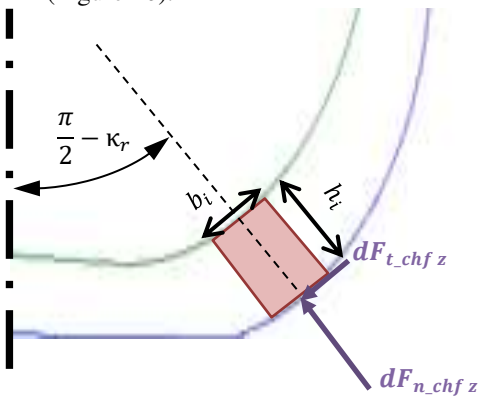

Figure 10: Elementary forces applied on the chamfer.

It can be noted that the direction of the elementary normal force $dF_{n\_chf\,z}(\varphi_i)$ and of the elementary tangential force $dF_{t\_chf\,z}(\varphi_i)$ vary along the chamfer, according to the evolution of the local tool cutting edge angle κ_r.

The elementary forces are then summed along the chamfer to obtain the total cutting forces applied on the radial part of the tooth "z" in position φ_i.

$$\begin{cases} F_{c\_chf\ z}(\varphi_i) = \sum_{r_{Ai}=Rt-Rb}^{Rt} dF_{c\_chf\ z}(r_{Ai},\varphi_i) = K_{c\_chf}.\sum_{r_{Ai}=Rt-Rb}^{Rt} h_i(r_{Ai},\varphi_i)^{1-q_{c\_chf}}.b_i(r_{Ai},\varphi_i) \\ F_{n\_chf\ z}(\varphi_i) = \sum_{r_{Ai}=Rt-Rb}^{Rt} dF_{n\_chf\ z}(r_{Ai},\varphi_i) = K_{n\_chf}.\sum_{r_{Ai}=Rt-Rb}^{Rt} h_i(r_{Ai},\varphi_i)^{1-q_{n\_chf}}.b_i(r_{Ai},\varphi_i) \\ F_{t\_chf\ z}(\varphi_i) = \sum_{r_{Ai}=Rt-Rb}^{Rt} dF_{t\_chf\ z}(r_{Ai},\varphi_i) = K_{t\_chf}.\sum_{r_{Ai}=Rt-Rb}^{Rt} h_i(r_{Ai},\varphi_i)^{1-q_{t\_chf}}.b_i(r_{Ai},\varphi_i) \end{cases} \quad \text{(eq.16)}$$

These forces $F_{c\_chf\ z}(\varphi_i)$, $F_{n\_chf\ z}(\varphi_i)$ and $F_{t\_chf\ z}(\varphi_i)$ are calculated for each tooth of the tool (Figure 11).

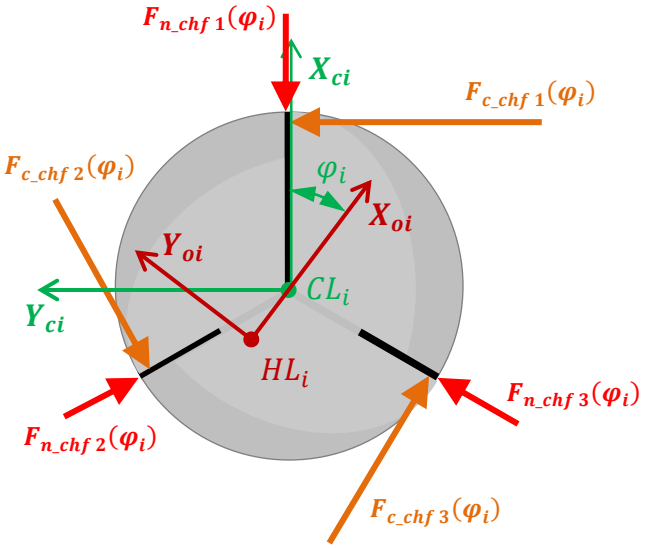

Figure 11 : Representation of forces generated on the radial part of a tool with three teeth (forces $F_{n\_chf\ z}(\varphi_i)$ are brought back into the plane of the figure and forces $F_{t\_chf\ z}(\varphi_i)$ are not shown).

For each tooth, the cutting force $F_{c\_chf\ z}(\varphi_i)$ applied on the radial part is normal to the chip section. Due to a local rake angle which is null, this force is included in the plane $(\boldsymbol{X_{ci}};\boldsymbol{Y_{ci}})$, or $(\boldsymbol{X_{oi}};\boldsymbol{Y_{oi}})$. The normal edge force $F_{n\_chf\ z}(\varphi_i)$ is included in the plane perpendicular to the cutting force $F_{c\_chf\ z}(\varphi_i)$, and nearly to be locally perpendicular to the edge. The tangential edge force $F_{t\_chf\ z}(\varphi_i)$ is also included in the plane perpendicular to the cutting force $F_{c\_chf\ z}(\varphi_i)$, and nearly to be locally tangent to the cutting edge.
As for the axial part, the modelling of the forces applied on the radial part of the tool considers 6 radial cutting parameters to be identified.

The proposed modelling expresses the local cutting forces for each tooth of the tool. The axial part and the radial part of the tool have been dissociated in order to take into account different cutting phenomena that occur under the tool tip and on the chamfer. The parameters of the modelling have to be identified separately for both parts, in order to be able to simulate the global forces generated in orbital drilling.

3.3. Experimental setup and calibration procedure

In this paper, the case of a three-flute tool (Z=3) of diameter D_t=9mm, with a corner radius R_b=1mm, and with a single tooth with center-cut (R_{cc}=2.2mm) is presented. The machined material was titanium alloy TiAl6V4 of 19mm thick. The identification of the model parameters "K" and "q" needs calibration tests to be conducted, respectively for the axial part and for the radial part of the tool. These calibration tests were performed on a DMG DMU50eVo CNC machining centre, equipped with a 24000rpm/25kW spindle. Once the model was identified, its validation was done by comparing simulated forces and measured forces in orbital drilling. The associated orbital drilling tests (borehole diameter D_h=11.1mm) were performed on a specific drill bench equipped with an orbital spindle, property of AIRBUS. For all tests (calibration and validation), cutting forces were recorded using the 6-component Kistler 9257B dynamometer and sampled at 10 kHz. The cutting conditions were variable for

the experimental plan. Only the cutting speed V_c was kept at a constant value of 30m/min (prescribed by the tool manufacturer to ensure the maximum tool life) as its influence on the cutting forces is negligible for small variations [4].

All the identified coefficients are summarized in Table 3. It is difficult to compare these coefficients directly as different cutting mechanisms are involved and different chip thicknesses are encountered. In order to compare the results of the calibration phase, the equivalent coefficients $K_c{}^*$ and $K_n{}^*$ are calculated for a given value of h from (eq.10). It appears that the coefficients for the radial part of the tool are nearly twice as important as for the axial part. This can be explained by the differences in terms of cutting geometry. On the radial part and on the axial part of the tool, the rake and clearance angles are different. Moreover, the edge sharpness may also be different. But also, the cutting speed may explain a part of this difference. It can be also noted that coefficients $K_c{}^*$ and $K_n{}^*$ are nearly equal for a given part of the tool. This expresses the importance of normal edge forces in orbital drilling, while cutting forces normal to the chip section are often considered as preponderant. The influence of the edge sharpness must also be considered.

	K_c	q_c	$K_c{}^* = K_c.h^{-q_c}$ (h =0.01mm)	K_n	q_n	$K_n{}^* = K_n.h^{-q_n}$ (h =0.01mm)	K_{ind}.s	q_{ind}
Radial Part	1643	0.229	4590	446	0.483	4124	-	-
Axial Part	192.79	0.577	2750	48.505	0.811	2010	2.5887	1

Table 3: Summary of the identified coefficients.

Since the models for the axial and the radial parts of the tool are calibrated, the global cutting forces can be simulated, analysed and compared to experimental measurements.

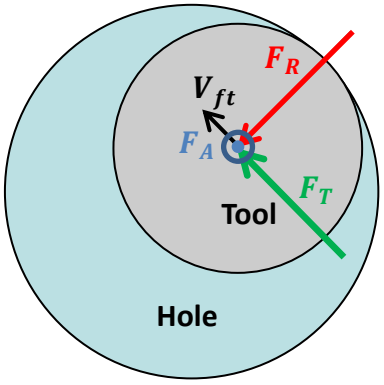

Figure 12: Global cutting forces on the tool

3.4. Result of the cutting forces modelling

First, from the identified coefficients, it is possible to simulate the forces applied on the axial part of the tool, considering the same parameters for the three teeth. For this, the forces F_{c_tip} and F_{n_tip} are firstly projected along the axis $\boldsymbol{Y_{oi}}$, $\boldsymbol{X_{oi}}$. The resulting forces are respectively F_{T_tip} (tangent to the borehole, along $\boldsymbol{Y_{oi}}$) and F_{R_tip} (radial to the borehole, along $-\boldsymbol{X_{oi}}$). The axial force F_{A_tip} is obtained by adding the projection of F_{n_tip} along axis $\boldsymbol{Z}$ and the indentation force F_{ind} (Figure 12):

$$\begin{cases} F_{T\_tip} = \sum_{z=1}^{Z} \left[\boldsymbol{F_{c\_tip\,z}}.\boldsymbol{Y_{oi}} + \boldsymbol{F_{n\_tip\,z}}.\boldsymbol{Y_{oi}} \right] \\ F_{R\_tip} = -\sum_{z=1}^{Z} \left[\boldsymbol{F_{c\_tip\,z}}.\boldsymbol{X_{oi}} + \boldsymbol{F_{n\_tip\,z}}.\boldsymbol{X_{oi}} \right] \\ F_{A\_tip} = \sum_{z=1}^{Z} \left[\boldsymbol{F_{n\_tip\,z}}.\boldsymbol{Z} \right] + F_{ind} \end{cases} \quad \text{(eq.17)}$$

In the same manner, the forces F_{c_chf} and F_{n_chf}, applied on the radial part of the tool, are simulated and projected along the axis $\boldsymbol{Y_{oi}}$, $\boldsymbol{X_{oi}}$ and $\boldsymbol{Z}$. The resulting forces are respectively F_{T_chf} (tangent to the borehole, along $\boldsymbol{Y_{oi}}$), F_{R_chf} (radial to the borehole, along $-\boldsymbol{X_{oi}}$) and F_{A_chf} (axial force, along $\boldsymbol{Z}$) (Figure 12):

$$\begin{cases} F_{T\_chf} = \sum_{z=1}^{3} \left[\boldsymbol{F_{c\_chf\ z}} . \boldsymbol{Y_{oi}} + \boldsymbol{F_{n\_chf\ z}} . \boldsymbol{Y_{oi}} \right] \\ F_{R\_chf} = -\sum_{z=1}^{3} \left[\boldsymbol{F_{c\_chf\ z}} . \boldsymbol{X_{oi}} + \boldsymbol{F_{n\_chf\ z}} . \boldsymbol{X_{oi}} \right] \\ F_{A\_chf} = \sum_{z=1}^{3} \left[\boldsymbol{F_{n\_chf\ z}} . \boldsymbol{Z} \right] \end{cases} \quad \text{(eq.18)}$$

$$\begin{cases} F_T = F_{T\_tip} + F_{T\_chf} \\ F_R = F_{R\_tip} + F_{R\_chf} \\ F_A = F_{A\_tip} + F_{A\_chf} \end{cases} \quad \text{(eq.19)}$$

The precise angular position of the tool in the borehole during drilling (θ_i) can be easily calculated. But experimentally, this angular position is difficult to measure during a drilling test. Therefore, the simulation of the cutting forces along $\boldsymbol{X}$ and $\boldsymbol{Y}$ axis cannot be compared to experimental results as the shift angle cannot be identified. For this reason, the comparison between the modelling and the measurements were based on the resultant force applied on the tool in the plane perpendicular to its axis (noted F_{xy}) and on the axial force F_z. From the measurements, F_{xy} can be calculated with the measured forces F_x and F_y:

$$F_{xy} = \sqrt{{F_x}^2 + {F_y}^2} \quad \text{(eq.20)}$$

The measured forces F_{xy} and F_z can be respectively compared to simulated forces F_{RT} and F_A, where:

$$F_{RT} = \sqrt{{F_R}^2 + {F_T}^2} \quad \text{(eq.21)}$$

The comparison between simulations and experimental measurements is performed considering the tool fully engaged into the material. The evolution of the cutting forces during the entry phase of the tool into the material would have been different but it has an insignificant influence on tool behaviour and on hole quality. Thus in the paper, this entry phase is not presented.
The measured cutting forces are firstly presented for a complete orbital revolution (Figure 13). It corresponds approximatively to 55 tool revolutions and 3s. An analysis of the signals in the frequency domain is also presented. It appears that the force evolution is stable. More, F_{xy} vary at a frequency equal to the tool revolution frequency (17,7Hz), while the axial force signal F_z present a frequency three times greater (53Hz). This validates the observations made earlier on simulations.

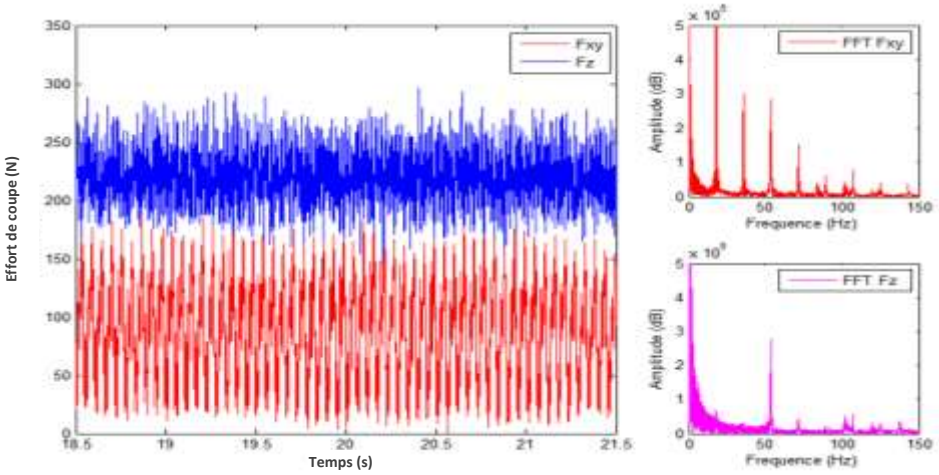

(a) *(b)*

Figure 13 : (a) Cutting forces measurements during orbital drilling (V_c=30m/min; f_{za}=0.005mm/tooth; f_{zt}=0.04mm/tooth); (b) analysis of force signals in the frequency domain.

The observed frequencies permit to compare simulations to experimental measurements only on a few tool revolutions. Three tool revolutions are presented (Figure 14).

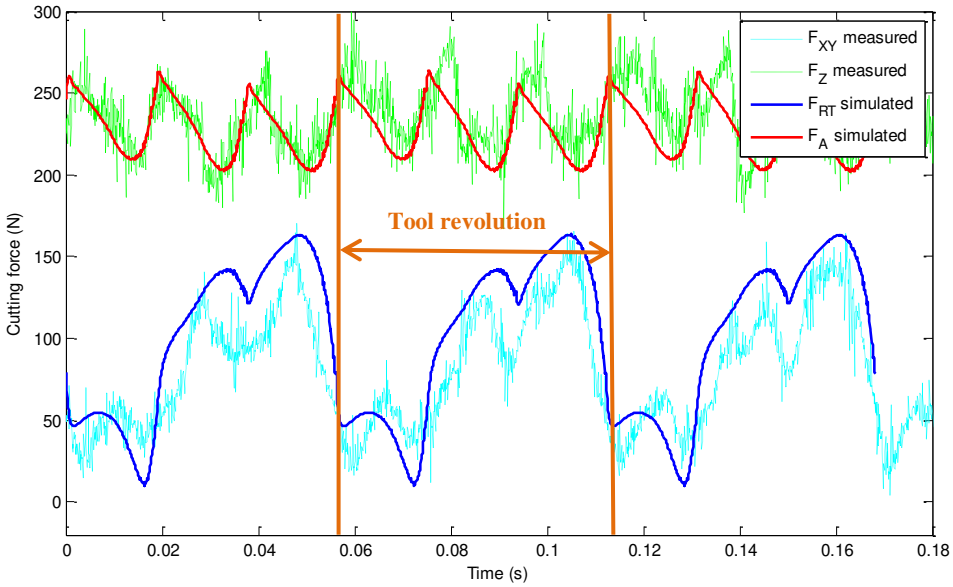

Figure 14: Comparison of simulated and measured cutting forces. V_c=30m/min; f_{za}=0.005mm/tooth; f_{zt}=0.04mm/tooth.

It can be noted that the simulated axial force F_A represents with a good fidelity the axial forces generated in orbital drilling. The edge passing frequency is found. Moreover, the amplitude of the axial force is really close to the measured one F_z.
The simulation of the resultant force F_{RT} shows also very good results. The characteristic evolution of this force is found, in relation with the evolution of F_T and F_R explained above. On the measurement of F_{xy}, the two characteristic frequencies clearly appear. So the proposed model permits to represent and to explain the specific evolution of this bending force (in a plane perpendicular to the axis of the tool). Moreover, the amplitude of this effort is well predicted, which validates the modelling and the identification of the cutting parameters.
As a result, the error between simulation and experimental results was assessed through Bravais-Pearson correlation coefficients R_{RT} and R_A. For the transversal cutting force F_{RT} the coefficient R_{RT} is 0.89. The mean error is 15N, corresponding to 18.8%. This percentage is relatively high because of the low values of the cutting force. For the axial cutting force F_A the coefficient R_A is 0.67. The mean error is 12N, corresponding to 5.3%. These results reflect a high correlation between simulation and experimental results. The proposed modelling permits a good estimation of the forces generated in orbital drilling and can be used for the optimization of the process now.

4. Influence of tool geometry

4.1. Influence of the geometry on the simulated cutting forces

Using a model, it is possible to simulate the cutting forces for different tool geometries and thus study the influence of this geometry on the forces. The goal is to link the geometry of the tool with the dimensional quality of the hole. This work will therefore focus on the forces having an impact on the final diameter of the hole and therefore partly on the geometric quality of the hole.
The forces having an impact on the machined diameter are the forces that tend to bend the tool as a tooth is making the surface of the hole. It was therefore chosen to study the force F_R when each tooth is machining the surface of the hole. Thus, a force is calculated for each tooth, the force (F_{RZ1}) is calculated when the tooth Z1 is in contact with the surface of the hole by taking into account the radial force F_R averaged over the area shown in **Error! Reference source not found.**. This zone is centered on the position where the tooth is in contact with the surface and represents 5° on each side of this position.

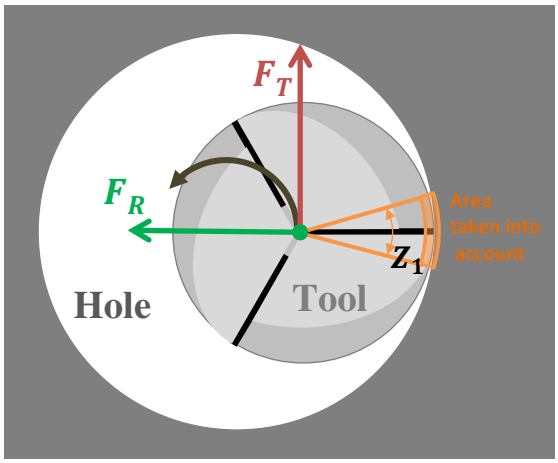

Figure 15 Area taken into account for the calculation of the effort F_R

Thus an F_{RZi} force is obtained for each tooth. It is considered that the final surface of the hole is made by the tooth with the least effort because it is the tooth that will flex the least. It is therefore this effort (F_{RZmin}) that will be used to compare the different geometries. Different tool geometries will be tested. For these simulations, the cutting conditions used are: V_c=30m/min; f_{za}=0.005mm/tooth; f_{zt}=0.04mm/tooth.

As the geometry of the tool is complex, only a few characteristic points will be studied. First, modeling will be used, by varying the geometry of the tool at the level of the axial zone of the tool, because in these works this zone is quite problematic. It could be identified that the tooth with the cut in the center was particularly fragile and wore very prematurely during the first holes. It is therefore interesting to study the utility of this center cut and the impact it has on drilling.

Figure 16 Tooth wear with center cut t

The cutting area near the tool center is always a problem area in tools machining at the end of the tool because the cutting conditions at this location are greatly degraded by the very low or zero cutting speed. Regarding orbital drilling, it is easy to calculate the real cutting speed (V_{C_real}) by taking into account the combination of the two rotations (N and N_{orb}):

$$V_{C\_real}(r_{Ai}, \varphi_i) = r_{Ai} \times 2\pi \times N - r_{ki}(r_{Ai}, \varphi_i) \times 2\pi \times N_{orb} \times \cos(\pi - \alpha(r_{Ai}, \varphi_i) - \varphi_i) \quad \text{(eq.22)}$$

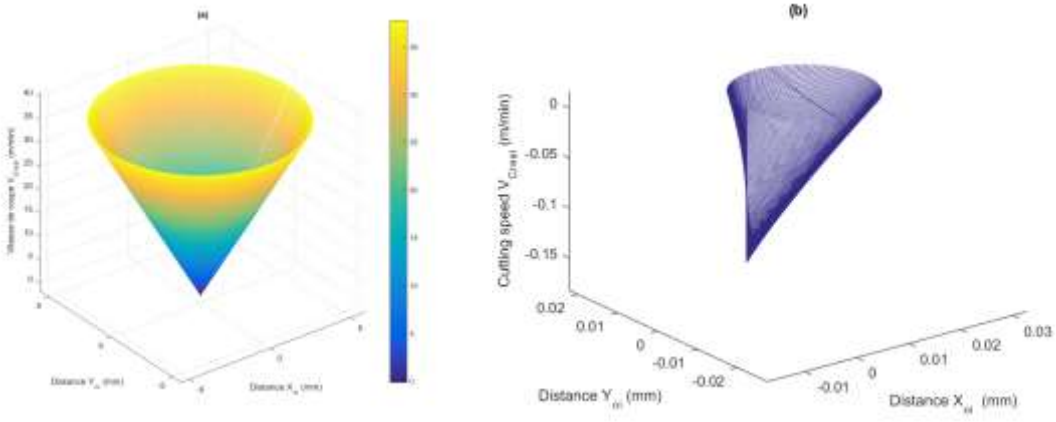

Figure 17 Cutting speed evolution during orbital drilling (a : all the tool ; b : locating on the tool center)(N=1100 tr/min; N_{orb}=21 tr/min)

And thus plot the evolution of the cutting speed along the cutting edge on a tool lathe (Figure 17-a), this result shows the cutting speed tending towards a zero value near the center of the tool as is the case with axial drilling. However, by analyzing more precisely the area near the center of the tool, the cutting speed becomes negative (Figure 17-b) due to the combination of the rotation of the tool and the orbital rotation. In the case of orbital drilling even if the orbital rotation seems negligible on the value of the rotation speed of the tool, it can still have an impact on the deterioration of the cutting conditions in the center of the tool.

It is therefore normal that the axial zone is also problematic in orbital trimming. Using the model, different tool geometries will be simulated to see the possibility of eliminating or reducing the material to be machined in this sensitive area. The first simulations consist in simulating material removal with a tool without a cut in the center, so all the teeth will have a similar profile with a non-cutting radius at the center R_{cc}.

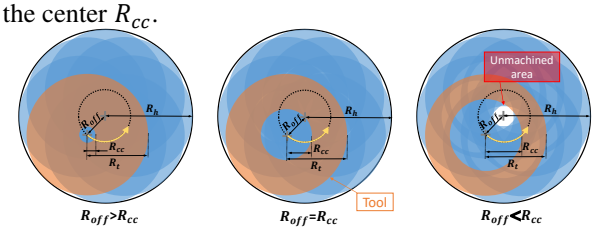

Figure 18 : Simulation of material removal for different values of the radius without center-cut

The simulation of the trace left by the rotation of the tool shows a maximum non-cutting radius equal to the interpolation R_{off} radius. It is therefore essential to keep a non-cutting radius at the center lower than the R_{off} radius to ensure that the cutting part can perform all of the machining. This non-cutting radius varies for the study between 0 mm and 1.5 mm (R_{off}) for a tool without a cut in the center. $R_{cc} = [0; 0{,}5; 1; 1{,}5]$ For simulations with a tool having a center cut, the non-cutting radius varies between 0 and 2.5 mm $R_{cc} = [0; 0{,}5; 1; 1{,}5; 2; 2{,}5]$. Because there is a tooth with a cut in the center, it is possible to have a non-cutting radius (R_{cc}) greater than the interpolation radius (R_{off}).

The other characteristics of the tool geometry remain identical to the tool used previously. A three-flute tool (Z=3) of diameter D_t=9mm, with a corner radius R_b=1mm, and with a tool cutting edge angle κ_r=93°.

The bending force (F_{RZmin}) is simulated for the different tool geometries with the following cutting conditions: V_c=30m/min; f_{za}=0.005mm/tooth; f_{zt}=0.04mm/tooth.

The result of all these simulations is presented in Figure 19. These graphs show that in general the increase of the tool cutting edge or of the radius without center-cut leads to a decrease in the bending force F_{RMIN}. In the case of a tool with a center cut, these variations are very significant, they go from 77N to -12N. This negative bending force means that all of the cutting forces generated by the three teeth tend to push the tooth machining the surface of the hole towards it. For the case of a tool without a center cut, these variations are less important, the bending force goes from 77N to 31N and therefore never becomes negative.

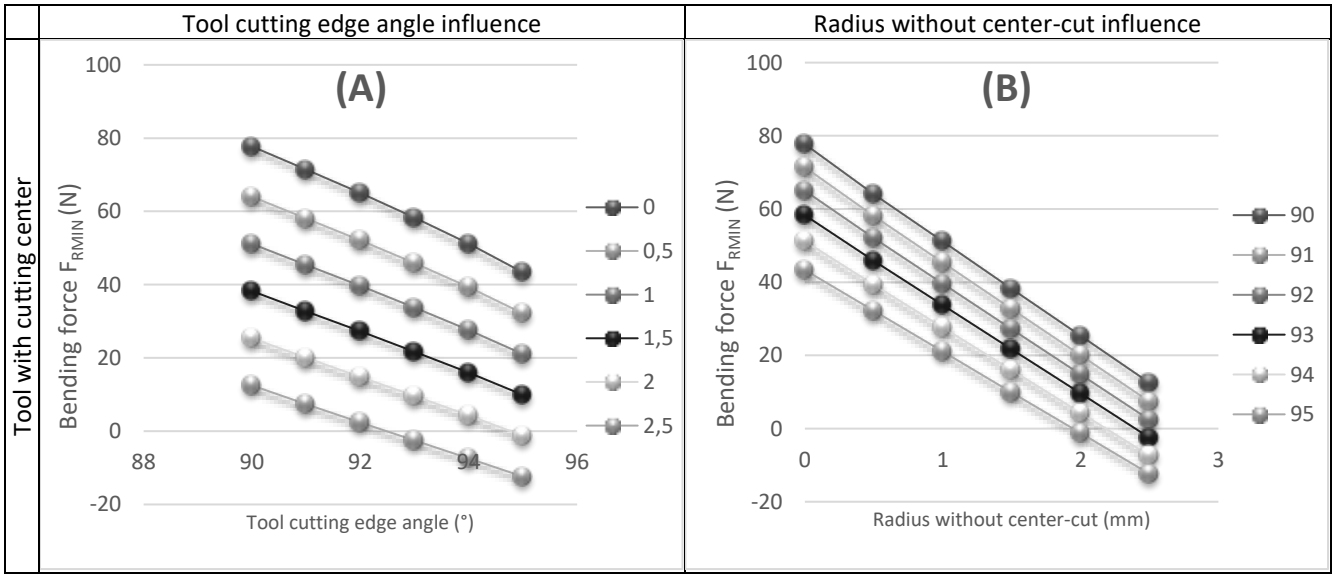

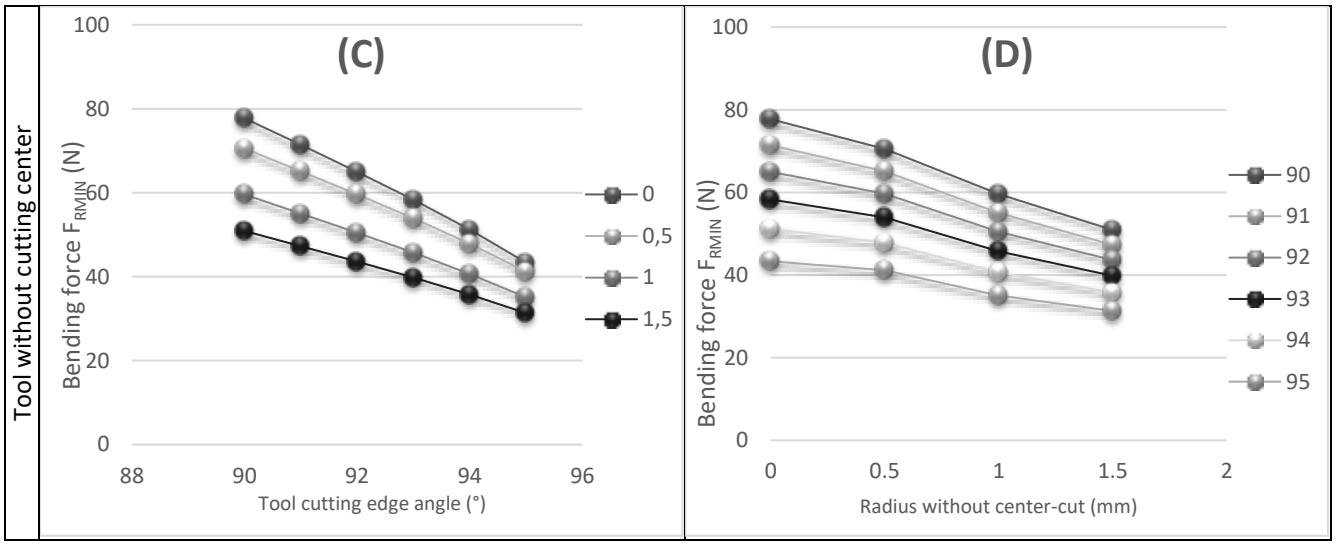

Figure 19 : Modeling results for the different geometries

To understand this result, we must be interested in the influence of these parameters on the evolution of the geometry of the chip of the axial part. The increase in radius without center-cut or the presence of teeth with center-cut, significantly modifies the geometry of the chip (Figure 20). In Figure 20-a the increase in the non-cutting radius causes an increase in the section of the chip section at the back of the tool and a decrease in the chip section at the front of the tool. The presence of a cut in the center has the same effect by increasing the chip section at the back of the tool (Figure 20-b). However, by working by down-milling, the forces generated by the machining of the back part of the tool are oriented so as to push the tool towards the surface of the hole and therefore counter the bending forces generated by the radial part of the tool. It's a reason why the minimal bending force decreases as the radius without center cut increases (Figure 19-B-D).

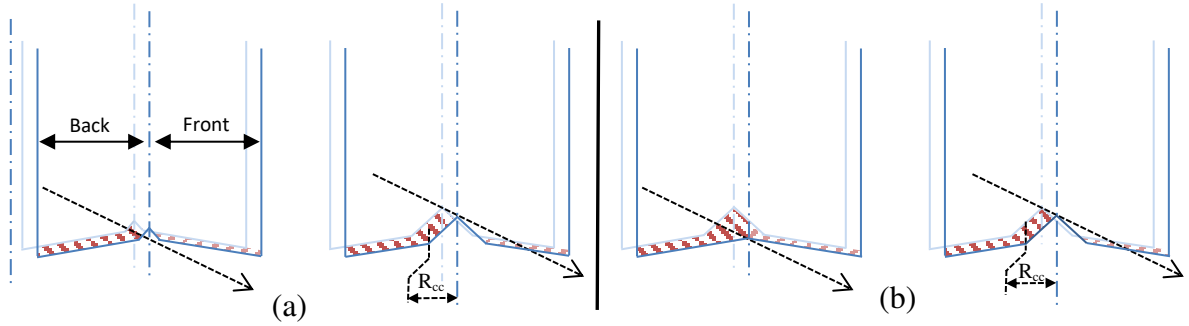

Figure 20 : Influence of the radius without center-cut (a) and the presence of the cutting center (b) on the geometry of the axial chip

The other parameter studied with the simulation is the tool cutting edge angle κ_r.

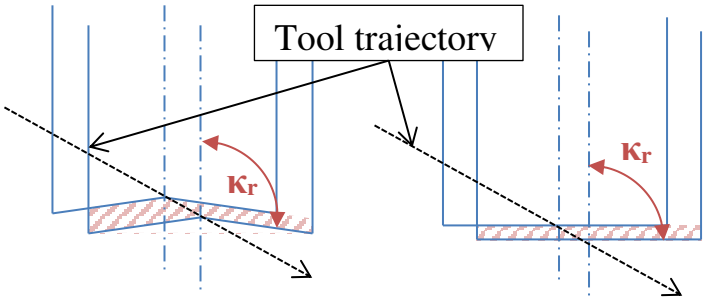

Figure 21 : Influence of the tool cutting edge angle κ_r on the geometry of the axial chip

Figure 21 shows the influence of the tool cutting edge angle on the chip section and as with the other two parameters discussed previously, the chip section at the back of the tool increases as the tool cutting edge angle increases.

It is therefore normal that the simulation shows a reduction in the minimal bending force when the tool cutting edge angle increases (Figure 20-A-C) for the same reasons.

In Figure 14, the measured force Fxy and the modeled force Frt show the successive passage of three teeth over the revolution of the tool. This is explained by the fact that the radial chip is not constant over the revolution of the tool. However, the differences between the peaks come from the presence of a single tooth with a central cut which causes a disturbance on the revolution of the explaining tool. Thanks to the modeling it is possible to study the evolution of the cutting force to better understand the phenomena generated by the geometry of the axial part of the tool. The tool performance and the cutting phenomena caused by the radial part of the tool are known and already considerably studied in the literature. The cutting phenomena of the axial part are more complex due to the combination of the geometry of the tool tip and the complex tool path.

To better understand the mechanisms during drilling, the evolution of the tangential force F_t at the contact point tool / work piece (according to $\mathbf{Y_{oi}}$) and of the radial force F_r (Figure 22) are modeled only for the axial part.

during one revolution of the tool, these two forces oscillate strongly, which means that the bending force is itself highly variable. So a dynamic phenomenon is established and must be study to understand the chip thickness of the radial cut. The Figure 22 shows that when the tooth with center cut is located in the "A" area ($0 < \varphi < \frac{\pi}{2}$), the radial force and tangential force are positive but quite low, not causing a significant modification in radial section.

When the tooth with center cut (z_1) is located in the "B" area ($\frac{3\pi}{2} < \varphi < 2\pi$), the radial force and tangential force are positive. Therefore, this resultant force tends to push the tooth being machined towards the surface.

When the tooth with center cut is located in the area "C", the radial force is positive and tangential force is negative. Therefore, this resultant force tends to push the tooth (z_2) towards hole surface and in reverse tends to withdraw the tooth (z3) of hole surface.

And when the tooth with center cut is located in the area "D", the radial and tangential force are negatives. Therefore, this resultant force tends to withdraw the tooth (z3) of hole

The hypothesis is that the radial section isn't homogeneous for the three teeth, because bending forces are different to each passage of various teeth on the radial cut area. The radial chip thickness machined by the tooth z_2 is greater than that machined by the tooth z_3.

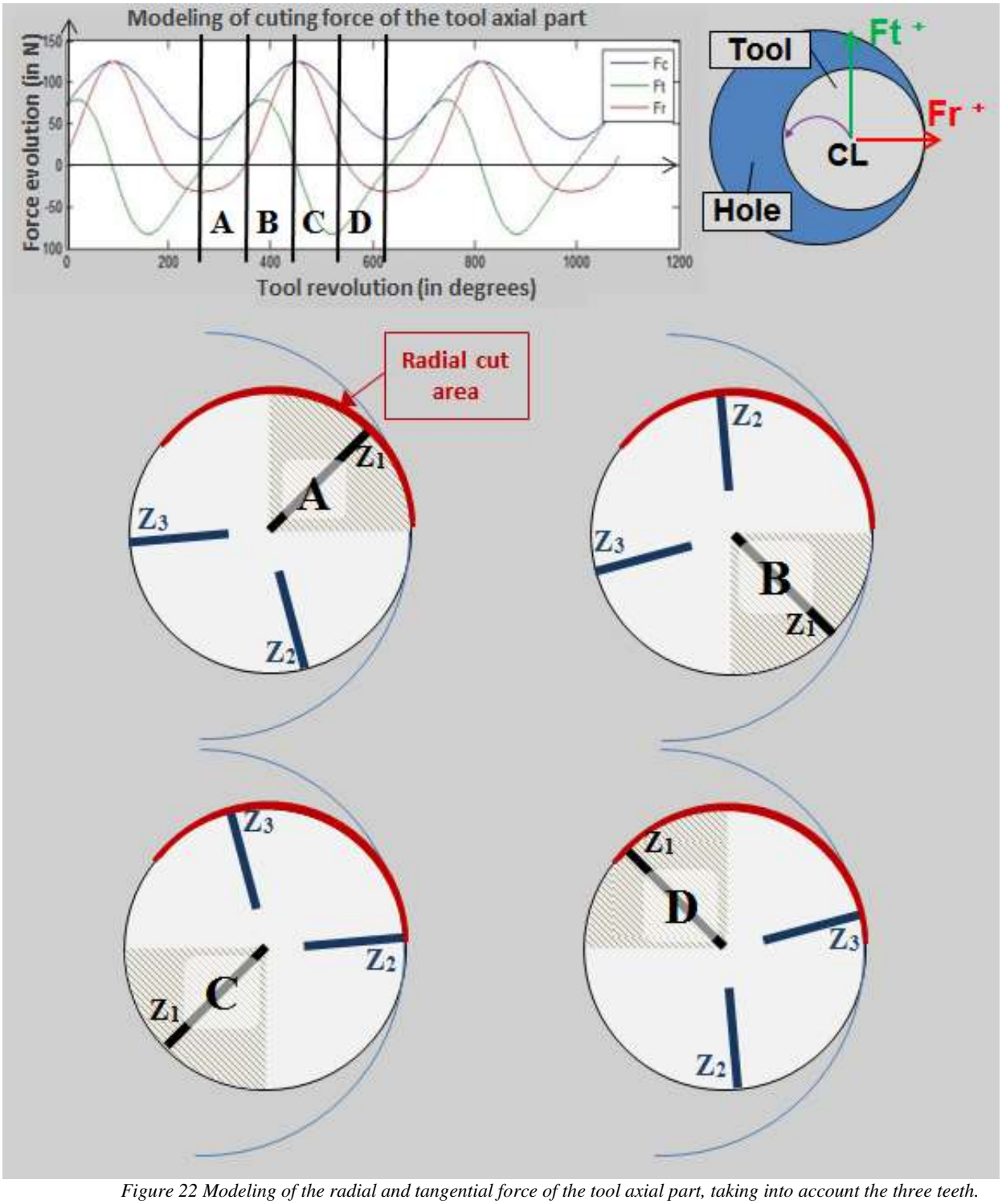

Figure 22 Modeling of the radial and tangential force of the tool axial part, taking into account the three teeth.

Results and discussions

To validate these observations on the simulation, tests were carried out. These tests are performed on a drill bench equipped with an orbital spindle. The cutting forces are recorded using the dynamometer Kistler and sampled at 10 kHz. A taring is performed on the signals obtained when measuring.

The hole diameter is 11.11mm and it is made with the same tool which has diameter of 9mm.

Three different geometry tools are tested (Figure 23). Only the axial part is different. The first tool is the tool previously studied with tool cutting edge angle ($\kappa_r = 93°$), one teeth with cutting tool center and the others with a radius without center cut $R_{cc} = 2mm$. The second tool is a similar tool, only the tool cutting edge angle is different. The axial part of the second tool is flat so $\kappa_r = 90°$. The third is the same than the second without the cutting tool center.

Tool N°1	*Tool N°2*	*Tool N°3*
κr=93°	**κr=90°**	**κr=90°**
With cutting tool center		Without cutting tool center
		

Figure 23 : The different geometry tool

For comparison of the three tools, cutting conditions have remained the same and are the conditions recommended by the manufacturer: V_c=30m/min; f_{za}=0.005mm/tooth; f_{zt}=0.04mm/tooth.

In order to bring out this dynamic phenomenon, a series of holes is created with each tool, with the similar conditions (material, cutting parameters, hole diameter) for each tool. And then the diameters of the holes will be measured on the three-dimensional measuring machine (MMT).

Tool N°1	*Tool N°2*	*Tool N°3*
κr=93°	**κr=90°**	**κr=90°**
With cutting tool center		Without cutting tool center
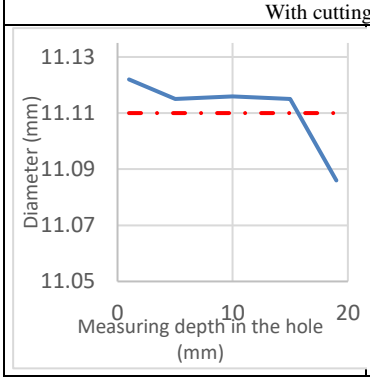	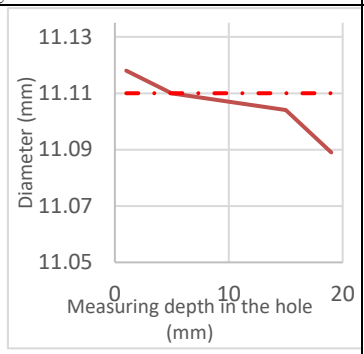	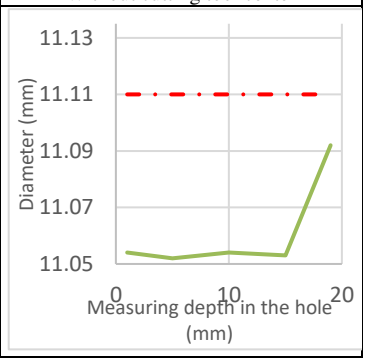

Figure 24 : Average profile measured on the hole for each tool

These measurements (Figure 24) show that with same cutting conditions the profile of the hole can be different. And especially that the axial part of the tool is very important on the profile, therefore on the bending tool.

On the profile of the first tool the entrance hole diameter is larger than output. This validates the result of the modeling of the cut (Figure 22) that the cut of the axial part of the tool causes a positive average radial force, increasing the hole diameter. And at the end of the drilling there is no cutting of the axial part therefore the diameter of the hole decreases.

Between the profile of the first tool and the second, only the tool cutting edge angle is different. The influence of this angle on the axial chip is showed on the Figure 21.

Therefore, the axial chip for the second tool is more homogeneous, which can be seen also on the modeling effort (Figure 25). The maximum radial force modeled for the second tool is 100N whereas for the first tool it's 150N, it's a reason why the variation of hole diameter is less important for the second tool

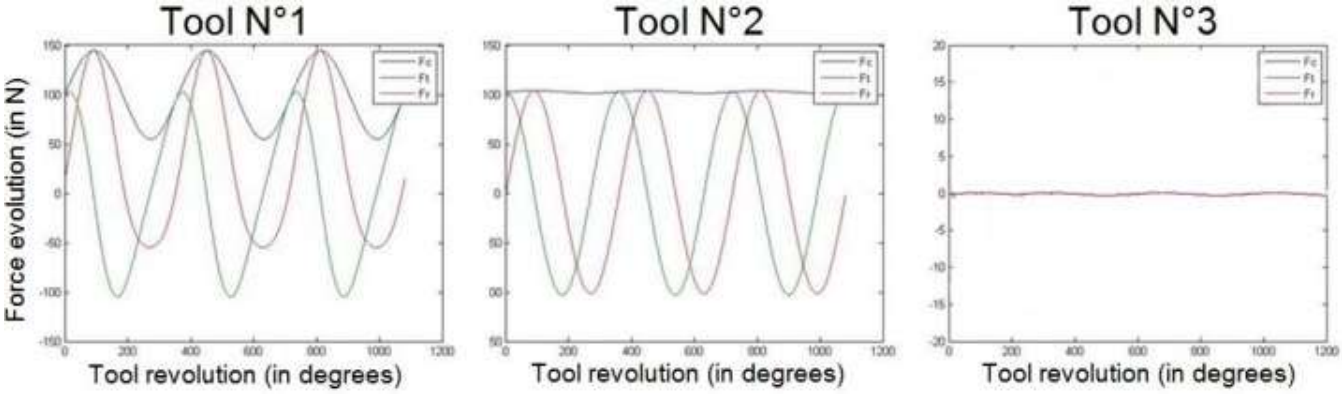

Figure 25 : Modeling of the cutting force of the tool axial part for the three tools

As regards the third tool, the three teeth are identical and the axial part is flat so the chip is identical for the three teeth. That is why the model shows no cutting force (Figure 25) because the forces on each tooth cancel each other.
Without the radial force generated by the axial part, the tool during the drilling bend and therefore realized a smaller diameter. The increase of diameter at the end of drilling, is due to the relaxation of the tool.
For tools n°1, n°2, and n°3, the F_{RMIN} force is respectively 9.5N, 25N, and 50N (Figure 19), which reflects an increasing bending for these tools and therefore a reduction in the drilled diameter. This is in agreement with the measurements carried out (Figure 24). The value of this force is difficult to use to predict the bending of the tool because it is important in this type of bending to take the dynamics into account. In addition, this force is extracted from a homogeneous cutting model over the whole of the axial part and comes from an estimate of a force at the center of the tool where the cutting conditions are strongly degraded for which the model has not been validated. However, this value appears to be an interesting criterion for optimizing the geometry of the tools and/or the cutting conditions in order to limit the bending of the tool.

5. Conclusions

In this paper, a new modelling of orbital drilling is proposed. Previous models available in the literature were developed for simple flat-end tools. But industrial tools used in orbital drilling are more complex and their geometry has a great influence on the process. However, a modelling considering a more complex tool geometry was not available, though it is necessary to reach an optimization in terms of tool design. In this paper, a model of chip geometry and cutting forces is proposed for complex tool geometries. The novelty is based on the integration of the tool geometry into the modelling, by considering local conditions and forces. The tool geometry is firstly expressed analytically, before being divided into elementary edge portions. On each portion, a local cutting force model is applied. The elementary forces are then summed, according to the evolution of the edge geometry. Finally, this model permits (i) to simulate the geometry of the chip, separately for the axial and for the radial parts of the tool, (ii) to simulate the cutting forces in relation to the tool geometry considered, including the important role of the shape of the axial part of the tool, and (iii) to dissociate the role of each part of the tool on the chip and forces generated, and so a better understanding of the cutting phenomena in orbital drilling (e.g. tool deflection).
To finish a study on the impact of the geometrical characteristics of the tool allowed to better understand the forces generated during the drilling and made it possible to link the geometry of the tool to the geometry of the drilling. A criterion has been developed in order to be able to carry out optimizations on the geometry of the tool but is also possible on the cutting conditions. In terms of applications, this model can be used to optimize the cutting conditions and the tool geometry in relation to the cutting forces generated (in direction and in amplitude). From the simulation of drilling defects due to the cutting forces (e.g. diameter decrease due to tool deflection), the model will permit to optimize the cutting conditions and/or the tool geometry in relation to the drilling quality.

6. Statements and Declarations

a. Funding

This work was carried out within the research project OPOSAP, funded by the region Midi-Pyrenees, the French state, and the European Commission. The work was also carried out within the context of the working group Manufacturing'21, which gathers 18 French research laboratories.

b. Conflicts of interest/Competing interests

The authors have no relevant financial or non-financial interests to disclose.

c. Availability of data and material

All data and materials are accessible.

d. Code availability

The codes developed in this work are custom codes.

e. Ethics approval

The authors fully approve the journal's ethics policy.

f. Author Contributions

All authors declare they have contributed to the study conception and design. Material preparation, data collection and analysis were performed by Pierre-Andre REY. The first draft of the manuscript was written by Pierre-Andre REY and all authors commented on previous versions of the manuscript. All authors read and approved the final manuscript.

7. References

[1] H. Tönshoff and W. Spintig, “Machining of holes: developments in drilling technology,” *Annals of the CIRP,* vol. 43, pp. 551-561, 1994.

[2] R. Lindqvist, I. Eriksson and M. Wolf, “Orbital drilling of sandwich constructions for space applications,” *Proceedings of the SAE Aerospace Automated Fastening Conference, Seattle, USA,* pp. 1-8, 2001.

[3] E. Brinksmeier, S. Fangmann and R. Rentsch, “Drilling of composites and resulting surface integrity,” *CIRP Annals - Manufacturing Technology,* vol. 60, pp. 57-60, 2011.

[4] B. Denkena, D. Boehnke and J. Dege, “Helical milling of CFRP–titanium layer compounds,” *CIRP Journal of Manufacturing Science and Technology,* vol. 1, no. 2, pp. 64-69, 2008.

[5] M. Ladonne, M. Cherif, Y. Landon, J.-Y. K'Nevez, O. Cahuc and C. De Castelabajac, “Modelling the vibration assisted drilling process: identification of influential phenomena,” *International Journal of Advanced Manufacturing Technology,* vol. 81, pp. 1657-1666, 2015.

[6] J. Le Dref, Y. Landon, G. Dessein and C. Espinosa, “Modelling kinematics and cutting forces in vibration assisted drilling,” *Mechanics and Industry,* 2015.

[7] A. L. Y. &. L. P. Araujo, «Smart drilling for Aerospace Industry: state of art in research and education,» chez *In 14th CIRP Conference on Intelligent Computation in Manufacturing Engineering*, Naples, 2020.

[8] R. Iyer, P. Koshy and E. Ng, “Helical milling: an enabling technology for hard machining precision holes in AISI D2 tool steel,” *International Journal of Machine Tools and Manufacture,* vol. 47, pp. 205-210, 2007.

[9] E. Brinksmeier and S. Fangmann, “Burr and cap formation by orbital drilling of aluminum,” *Proceedings of the CIRP, International Conference on Burrs, Kaiserslautern, Germany,* pp. 31-45, 2009.

[10] A. Sadek, M. Meshreki and M. Attia, “Characterization and optimization of orbital drilling of woven carbon fiber reinforced expoxy laminates,” *CIRP Annals - Manufacturing Technology,* vol. 61, pp. 123-126, 2012.

[11] E. Ezugwu et Z. Wang, «Titanium alloys and their machinability a review,» *Journal of materials processing technology,* vol. 68, n° %13, pp. 262-274, 1997.

[12] N. company, «Orbital drilling inventor,» 2018. [En ligne]. Available: https://novator.eu.

[13] D. Sun, P. Lemoine, D. Keys, P. Doyle, S. Malinov, Q. Zhao, X. Qin et Y. Jin, «Hole-making processes and their impacts on the microstructure and fatigue response of aircraft alloys,» *International Journal of Advanced Manufacturing Technology,* vol. 94, pp. 1719-1726, 2018.

[14] R. D. Pereira, L. C. Brandão, A. d. Paiva, J. Ferreira et J. P. Davim, «A review of helical milling process,» *International Journal of Machine Tools & Manufacture,* vol. 120, pp. 27-48, 2017.

[15] O. Ozturk, Z. Kilic et Y. Altintas, «Mechanics and dynamics of orbital drilling operations,» *International Journal of Machine Tools & Manufacture,* vol. 129, pp. 37-47, 2018.

[16] E. Brinksmeier, S. Fangmann and I. Meyer, “Orbital drilling kinematics,” *Production Engineering,* vol. 2, no. 3, pp. 277-283, 2008.

[17] P. Rey, J. LeDref, J. Senatore et Y. Landon, «Modelling of Cutting forces in orbital drilling of titanium alloy Ti-6Al-4V,» *International Journal of Machine Tools and Manufacture,* vol. 106, pp. 75-88, 2016.

[18] L. Zhou, H. Dong, Y. Ke et G. Chen, «Modeling of non-linear cutting forces for dry orbital drilling process based on undeformed chip geometry,» *International Journal of Advanced Manufacturing Technology,* vol. 94, pp. 203-216, 2018.

[19] L. Zhou, H. Dong, Y. Ke et G. Chen, «Analysis of the chip-splitting performance of a dedicated cutting tool in dry orbital drilling process,» *International Journal of Advanced Manufacturing Technology,* vol. 90, pp. 1809-1823, 2017.

[20] S. Segonds, Y. Landon, F. Monies and P. Lagarrigue, “Method for rapid characterisation of cutting forces in end milling considering runout,” *International Journal of Machining and Machinability of Materials,* vol. 1, no. 1, pp. 45-61, 2006.

[21] M. E. Merchant, “Mechanics of the metal cutting process,” *Journal of Applied Physics,* vol. 16, pp. 267-275, 1945.

[22] Y. Altintas and Z. Kilic, “Generalized dynamic model of metal cutting operations.,” *Annals of the CIRP - Manufacturing Technology,* vol. 62, no. 1, pp. 47-50, 2013.

[23] B. Denkena and J. Kôhler, “Consideration of the form of the undeformed section of cut in the calculation of machining forces,” *Machining Science and Technology,* vol. 14, no. 4, pp. 455-470, 2010.

[24] P. Lorong, A. Larue and A. Perez Duarte, “Dynamic study of thin wall part turning,” *Advanced Materials Research,* vol. 223, pp. 591-599, 2011.

[25] O. Kienzle and H. Victor, “Spezifische schnittkräfte bei der metallbearbeitung,” *Werkstattstechnik und Maschinenbau,* vol. 47, no. 5, pp. 224-225, 1957.

[26] R. Williams, «A study of drilling process,» *Journal of engineering for industry,* 1974.

[27] Y. Altintas and A. Ber, “Manufacturing automation: metal cutting mechanics, machine tool vibrations and CNC design,” *Applied Mechanics Reviews,* vol. 54, pp. 84-94, 2001.

[28] J. Tlusty and P. McNeil, “Dynamics of cutting forces in end milling,” *Annals of the CIRP,* vol. 24, pp. 21-25, 1975.

[29] W. Kline, R. DeVor and R. Lindberg, “The prediction of cutting forces in end milling with application to cornering cuts,” *International Journal of Machine Tool Design and Research,* vol. 22, pp. 7-22, 1982.

[30] E. Armarego and R. Whitfield, “Computer based modelling of popular machining operations for force and power prediction,” *Annals of the CIRP - Manufacturing Technology,* vol. 34, no. 1, pp. 65-69, 1985.

[31] A. Sabberwal and F. Koenigsberger, “Chip section and cutting force during the milling operation,” *Annals of the CIRP,* vol. 10, no. 3, pp. 62-66, 1961.

[32] M. Mousseigne, Y. Landon, S. Seguy, G. Dessein and J. Redonnet, “Predicting the dynamic behaviour of torus milling tools when climb milling using the stability lobes theory,” *International Journal of Machine Tools and Manufacture,* vol. 65, pp. 47-57, 2013.

[33] S. Engin and Y. Altintas, “Mechanics and dynamics of general milling cutters. Part I: helical end mills,” *International Journal of Machine Tools and Manufacture,* vol. 41, pp. 2195-2212, 2001.

[34] P. Rahme, Y. Landon, F. Lachaud, R. Piquet and P. Lagarrigue, “Delamination-free drilling of thick composite materials,” *Composites Part A: Applied Science and Manufacturing,* vol. 72, pp. 148-159, 2015.

[35] H. Hocheng and C. Dharan, “Delamination during drilling in composite laminates,” *ASME Journal of Engineering for Industry,* vol. 112, pp. 236-239, 1990.

[36] M. Ramulu, T. Branson and D. Kim, “A study on the drilling of composite and titanium stacks,” *Composite Structures,* vol. 54, pp. 67-77, 2001.

[37] J. Davim and O. Reis, “Damage and dimensional precision on milling carbon fiber reinforced plastics using design experiments,” *Journal of Materials Processing Technology,* vol. 160, pp. 160-167, 2005.

[38] A. Molinari, C. Musquar et G. Sutter, «Adiabatic shear banding in high speed machining of Ti6Al4V: experiments,» *International journal of Plasticity,* vol. 18, n° %14, pp. 443-459, 2002.

[39] E. Brinksmeier et R. Janssen, «Drilling of multi-layer materials consisting of carbon fiber reinforced,» *CIRP Annals - Manufacturing Technology,* vol. 51, pp. 87-90, 2002.